ACS Partner Journal

Journal of the American Society for Mass Spectrometry

pubs.acs.org/jasms

Article

Do Nanodisc Assembly Conditions Affect Natural Lipid Uptake?

Published as part of the Journal of the American Society for Mass Spectrometry virtual special issue "Focus: Next Generation Mass Spectrometry Omics Technologies".

Melanie T. Odenkirk, Guozhi Zhang, and Michael T. Marty*

Cite This: *J. Am. Soc. Mass Spectrom.* 2023, 34, 2006−2015

Read Online

ACCESS | Metrics & More | Article Recommendations | Supporting Information

ABSTRACT: Lipids play critical roles in modulating membrane protein structure, interactions, and activity. Nanodiscs provide a tunable membrane mimetic that can model these endogenous protein−lipid interactions in a nanoscale lipid bilayer. However, most studies of membrane proteins with nanodiscs use simple synthetic lipids that lack the headgroup and fatty acyl diversity of natural extracts. Prior research has successfully used natural lipid extracts in nanodiscs that more accurately mimic natural environments, but it is not clear how nanodisc assembly may bias the incorporated lipid profiles. Here, we applied lipidomics to investigate how nanodisc assembly conditions affect the profile of natural lipids in nanodiscs. Specifically, we tested the effects of assembly temperature, nanodisc size, and lipidome extract complexity. Globally, our analysis demonstrates that the lipids profiles are largely unaffected by nanodisc assembly conditions. However, a few notable changes emerged within individual lipids and lipid classes, such as a differential incorporation of cardiolipin and phosphatidylglycerol lipids from the *E. coli* polar lipid extract at different temperatures. Conversely, some classes of brain lipids were affected by nanodisc size at higher temperatures. Collectively, these data enable the application of nanodiscs to study protein−lipid interactions in complex lipid environments.

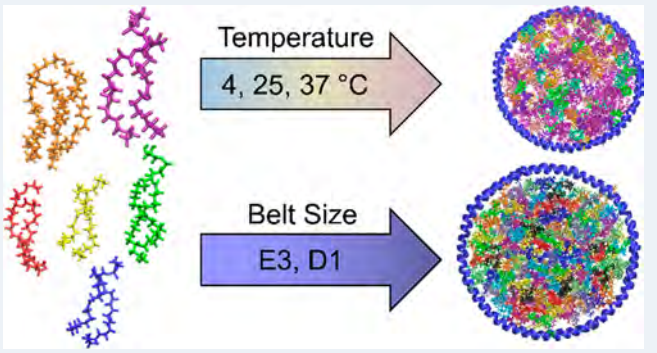

INTRODUCTION

Biological lipid membranes are heterogeneous and dynamic. In eukaryotes, membrane lipids span three prominent lipid categories (sphingolipids, glycerophospholipids, and sterols) that are further differentiated by class.[1] Conversely, bacterial lipidomes are primarily composed of glycerophospholipids and saccharolipids.[2] Variations in lipids can affect the physiochemical properties of biological membranes, such as the curvature or fluidity.[3−5]

Membrane proteins represent the largest category of pharmaceutical drug targets and have critical roles in cellular processes.[6] Increasing evidence indicates that lipids can be essential modulators of membrane proteins through direct and indirect interactions.[7−11] To preserve these protein−lipid interactions, lipoprotein nanodiscs provide a mimetic to solubilize membrane proteins in a tunable lipid environment.[12] Thus, nanodiscs provide useful platforms for drug screening and structural biology.[13−17]

Many studies of membrane proteins use nanodiscs formed from simple, synthetic mixtures containing a few lipid types.[18,19] Synthetic lipids provide an indispensable tool for tuning membrane properties and studying their effects. However, these synthetic lipid mixtures do not capture the full bilayer diversity and membrane characteristics that are critical for membrane protein interactions.[18−20]

To more effectively model natural membranes, early research[21] demonstrated that nanodiscs can be formed with natural lipid extracts. With thin layer chromatography (TLC) analysis, they did not observe major changes in the lipid class composition between the starting insect cell membranes and the lipid nanodiscs.[21] Since then, researchers have used natural lipid nanodiscs for a range of structural and functional studies of membrane proteins, including with a range of different types of extracts.[22−28] However, the lipidome of these natural lipid nanodiscs is often overlooked in these applications, so it is not clear how nanodisc assembly conditions may bias natural lipid uptake.

The lipidomic profile of polymer-encapsulated lipid nanoparticles, most notably styrene maleic acid lipid particles (SMALPs), have been somewhat more thoroughly studied.

Received: May 9, 2023
Revised: June 19, 2023
Accepted: July 21, 2023
Published: July 31, 2023

SMALPs provided a unique route to isolate lipids and membrane proteins directly from natural bilayers into lipid nanoparticles. Lipidomic analysis of membrane proteins isolated from SMALPs and related polymers has been used to identify lipids that bind tightly to membrane proteins in their native lipid environment.[29−32] Early research suggested that SMALPs do not seem to have prominent biases in lipid assembly,[31] but recent studies have revealed that lipid uptake can be affected by the polymer scaffold used.[33] Clearly, more research is needed to understand how natural lipids incorporate into lipid nanoparticles.

Here, we tested how lipoprotein nanodisc assembly conditions affect the uptake of natural lipid extracts. We chose assembly conditions that matched those most commonly used in the field. Because assembly temperatures are often selected to match lipid phase transition temperature (T_m) and enhance membrane protein stability,[34] we compared nanodisc lipid profiles across various assembly temperatures including cold (4 °C), room temperature (25 °C), and physiological conditions (37 °C). This span of temperatures encompasses the phase transitions for commonly used lipids,[35] and membrane proteins are often incorporated at either cold or room temperatures. We also compared how the diameters of the nanodisc influenced lipid uptake by investigating different belt sizes with MSP1D1 (D1, 9.7 nm) and MSP1E3D1 (E3, 12.9 nm).[35] We chose these two MSP belts because they are the most commonly used in the field and capture two distinct sizes. Finally, for all these assembly conditions, we consider two different natural lipid extracts, *E. coli* and brain polar lipid extracts, to model bacterial and mammalian lipidomes. The resulting changes of differential lipid uptake were determined to understand if/how nanodisc assembly conditions bias the uptake of lipids from natural lipid extracts.

METHODS

Sample Preparation. *E. coli* and porcine brain polar lipid extracts (Avanti Polar Lipids, Inc. Alabaster, AL, USA) were dissolved in chloroform, dried under nitrogen gas, and left overnight under vacuum. A single lot was used for consistency. Dried lipids were quantified by a Mettler Toledo XSE105 analytical balance. Lipids were then either resuspended in methanol for the curation of lipid libraries or a 0.1 M sodium cholate solution to a final lipid concentration of 50 mM for nanodisc assembly. This concentration was calculated based on an estimated 700 g/mol average molecular weight for the lipids. Although other detergents can be used in nanodisc assembly, we chose cholate because it is the most common. Membrane scaffold proteins MSP1D1 (D1) and MSP1E3D1 (E3) were expressed and purified as described previously, and polyhistidine tags were removed.[36−38] Triplicate replicates of nanodiscs were assembled overnight across various incubation temperatures (4, 25, and 37 °C) for each MSP belt. The MSP:lipid molar ratios were 1:60 and 1:110 for *E. coli* polar lipids with D1 and E3, respectively. Brain polar lipid nanodiscs were assembled with MSP:lipid molar ratios of 1:65 and 1:130 for D1 and E3, respectively. These ratios were determined empirically by starting with the recommended values[35] and making slight adjustments to optimize the assembly. Nanodiscs formed uniform assemblies, as confirmed by size exclusion chromatography.

Lipidomics. For lipidomic analysis, nanodiscs were diluted in methanol to a lipid concentration range of 0.1−1 μM. The EquiSPLASH (Avanti) internal standard supplemented with tetra-myristoyl-cardiolipin (TMCL) as a standard for the cardiolipin class was added to each sample to an approximate 1 μM final lipid concentration. Samples were then analyzed with a trap-and-elute RPLC-MS method. The RPLC separation of lipids was performed on a 2D Waters ACQUITY I Class chromatography system with an autosampler and column compartment maintained at 10 and 40 °C, respectively. For each separation, approximately 5−8 μL of lipid samples was injected and trapped on a Waters XBridge C8 Direct Connect HP (10 μm, 2.1 × 30 mm) followed by separation on a Waters ACQUITY Premier CSH C18 UPLC column (1.7 μm, 1 × 100 mm). The mobile phase consisted of 60/40 acetonitrile/water with 10 mM ammonium acetate (mobile phase A, MPA) and 90/10 isopropanol/acetonitrile with 10 mM ammonium acetate (mobile phase B, MPB).[39] The 21 min gradient elution method was run at a flow rate of 0.25 mL/min and is described in Table S1.

The eluent of HPLC separations were then introduced to a Waters Synapt XS mass spectrometer. Electrospray ionization of samples was performed in negative ion mode only for *E. coli* lipids and both negative and positive mode for brain lipids, performed as separate injections. For positive acquisitions, the cone gas flow rate was 10 L/h and capillary and sampling cone voltages were set to 2.2 kV and 45 V, respectively. In negative mode, these values were 30 L/h, −2.0 kV, and 40 V. For both modes, the source offset and temperature were set to 4 V and 120 °C, and the desolvation temperature and gas flow were 450 °C and 700 L/h. To ensure high mass accuracy and enhanced sensitivity of our analysis, all data were collected in resolution mode across 50−2000 m/z with a quad profile optimized above 440 m/z. Additionally, internal mass correction was applied through the simultaneous sampling of leucine enkephalin as the LockSpray reference molecule.

To build *E. coli* and brain polar lipid extract libraries, lipid extracts reconstituted in methanol were analyzed in triplicate with a data-dependent acquisition (DDA) method at a 0.1 s scan time. Specifically, we employed a FastDDA method that excluded precursor masses between 50−350 m/z with mass resolution of 4.7 and 15 for MS/MS selection at low and high mass ends. For each MS scan, seven ions were selected for fragmentation at a ± 100 ppm tolerance. Trap MS/MS collision energy ramps were applied at low mass (5−10 V, 50 m/z) while the high mass (2,000 m/z) was 70−150 and 75−155 V for positive and negative mode analyses. After building the libraries (described below), we performed quantitation using a simple MS1 acquisition at a scan rate of 0.5 s. Default trap and transfer collision energies were 4 and 2 V, respectively. Peaks were assigned using accurate mass and retention time matching.[40]

Data Processing, Statistical Analysis, and Visualization. To build a library of identified lipids, we used MS-DIAL (RIKEN Center for Sustainable Resource Science: Metabolome Informatics Research Team) version 4.9 for the analysis of FastDDA data files.[41] Following the alignment of technical triplicates, DDA data were matched to the LipidBlast reference library.[41,42] For each matching identification, lipids were manually validated based on mass error, MS2 coverage of fatty acyl and headgroup fragments, expected retention match, and overall match scores. Lipid candidates that lacked sufficient fragmentation data but were in otherwise good agreement were included at speciation levels to match identification confidence (i.e., PE 40:0 instead of PE 18:0_22:0 if there was insufficient fatty acyl fragments).

https://doi.org/10.1021/jasms.3c00170
J. Am. Soc. Mass Spectrom. 2023, 34, 2006−2015

The resulting library for *E. coli* included 55 lipids across phosphatidylethanolamine (PE), phosphatidylglycerol (PG), and cardiolipin (CL) phospholipid classes. Notably, the coverage of classes matched existing literature and therefore validates our methods.[43,44] The library of brain polar extract showed significantly more lipidome heterogeneity, spanning 3 categories and 12 lipid classes. As with *E. coli* lipid coverage, the 279 identified brain lipids reflected similar class coverage to the anticipated composition.[45,46]

After building the lipid libraries in MS-DIAL, transition lists were exported into Skyline (University of Washington), where accurate mass and time (AMT) matching was used to assign lipid identifications to MS1 acquisitions.[40,47] Lipid areas for all samples were exported from Skyline for the quantitation of relative area changes across nanodisc assembly conditions.

The processing and evaluation of differential uptake of lipids in various nanodisc assembly conditions was conducted in R (version 4.2.1, R Foundation) using the package pmartR.[48] First, data was $\log_2$ transformed and subsequently screened for outlier samples with Pearson correlation, principal component analysis, and robust Mahalanobis distance.[48] Additionally, any lipid signals that lacked quantitative reproducibility (absent in over 60% of samples) were removed. Following outlier exclusion, missing values were imputed for any lipid signals below the quantitation limit using the quantile regression imputation of left-censored data (QRILC) algorithm.[49]

Data were then normalized to the summed abundance of the identified lipid signals (mTIC). Statistical evaluations were then completed on this processed data using an unpaired ANOVA analysis. Significant lipid fluctuations were defined at a type one error rate of 95%. An additional Holm multiple comparisons correction was also applied to adjust *p*-values. Outputs from data processing and statistical analysis of *E. coli* and brain polar lipid extracts are presented in Tables S2−S3. To facilitate the visualization of data and define structural trends to differential lipid uptake, we also employed the SCOPE cheminformatics toolbox and Lipid Mini-on functional enrichment analysis.[50,51] All enrichment results are included in Table S4.

Class comparisons were performed in Python (Python Software Foundation) by normalizing the data to the internal standards for each class and then summing the normalized signal for each class. The total normalized class signal was then divided by the total normalized signal of all classes to get the mole percent for each class. For *E. coli* lipids, pairwise *t* tests were performed for selected classes and conditions. For brain lipids, changes for each class between belts and temperatures were independently tested with ANOVA or Welch ANOVA analysis (depending on a Levene test for equal variances). For conditions that were significant, posthoc testing was performed using either a Tukey or Games-Howell test. Outputs from class-based analyses are presented in Table S5.

RESULTS AND DISCUSSION

Here, we measured how the uptake of lipids from natural lipid extracts into nanodiscs is impacted by the assembly conditions. We considered how lipidome compositions are affected by two factors, assembly temperature and nanodisc size, that are commonly used to optimize nanodisc assembly for membrane protein integration.[34] Using a lipid library built from LC-DDA data, a total of 55 and 279 lipids were identified across *E. coli* and brain extracts, respectively. These lipids were then quantified for replicate nanodisc assemblies from MS1 acquisitions. From these comprehensive profiles of both bacterial and mammalian lipid compositions, we were then able to assess how lipid uptake in nanodiscs is differentially influenced by assembly conditions.

We first compared the global lipid profiles through differential clustering in PCA analysis for nanodiscs formed with *E. coli* polar lipid extract (Figure 1A). From the biological replicates analyzed for each condition, we observed no clear grouping of lipid compositions. Lipid profiles across assembly conditions also did not show clear grouping for nanodiscs formed from brain polar lipid extract (Figure 1B). Generally, both lipid extracts included global conservations of lipid profiles.

Nanodisc Assembly from *E. coli* Polar Lipid Extract. The lipid composition in the *E. coli* membrane maintains a balance between zwitterionic PE lipids and anionic PG and CL. We identified 55 lipids from *E. coli* that were categorized into 3 different classes: 16 CL, 16 PG, and 23 PE. PE lipids were further classified as 2 lyso-PE (LPE) and 21 PE lipids. This profile matched prior literature and the expected species.[43,44]

To gain a deeper understanding of nanodisc assembly effects on lipid uptake, we surveyed individual species and looked for class and fatty acyl trends to differential lipid uptake. In the following sections, we consider the variations across different nanodisc sizes and incubation temperature.

Effects of Nanodisc Size. To accommodate membrane proteins with different sizes, a variety of MSP belts have been designed to create nanodiscs with different diameters and therefore different numbers of lipids per complex.[35] There are several reasons why nanodisc size may trigger biased lipid composition. First, recent work has revealed that the bilayer may curve near the edge of nanodiscs, which may serve to enrich specific lipids in this peripheral zone.[52−54] Smaller D1 nanodiscs have a larger fraction of edge lipids than larger E3 nanodiscs. Additionally, lipids could organize into nanodomains or have lipid−lipid interactions that bias the lipid profile during assembly.[55]

To assess how nanodisc size affected the lipid profile, we performed lipidomic analysis on *E. coli* nanodisc made from either MSP1D1 (D1, 9.7 nm) or MSP1D1E3 (E3, 12.9 nm) belts, which were assembled at a ratio of 120 or 220 lipids per nanodiscs, respectively. Because lipid packing is affected by their fluidity, we also considered nanodisc size effects at different assembly temperatures of 4, 25, and 37 °C.

Analyzing differential lipid uptake in D1 versus E3 nanodiscs, 10 of the total 55 lipids (18%) were significantly different between belts at one or more temperatures (Figure 2A). Three lipids changed significantly between belt sizes (1 elevated in larger E3 nanodiscs, 2 elevated in smaller D1 nanodiscs) at 4 °C, 5 changed significantly (4 at greater levels in E3, 1 elevated in D1) at 25 °C, and 3 changed significantly (1 elevated in E3, 2 elevated in D1) at 37 °C.

Among the lipids that changed, only one lipid, PE 16:0/16:0, was repeatedly affected by belt size differences where it was first more incorporated in E3 belts at 25 °C and then more incorporated in D1 belts at 37 °C. Lyso-PE was most dramatically changed, but they lacked a clear trend. We interpret that challenges in quantifying lyso-PE, their inherent solubility, and/or dependence on lipid membrane structure might make them highly variable.[56] Overall, although individual lipids fluctuated, no major trends emerged that would suggest a systematic bias in incorporation. Instead, we

https://doi.org/10.1021/jasms.3c00170
J. Am. Soc. Mass Spectrom. 2023, 34, 2006−2015

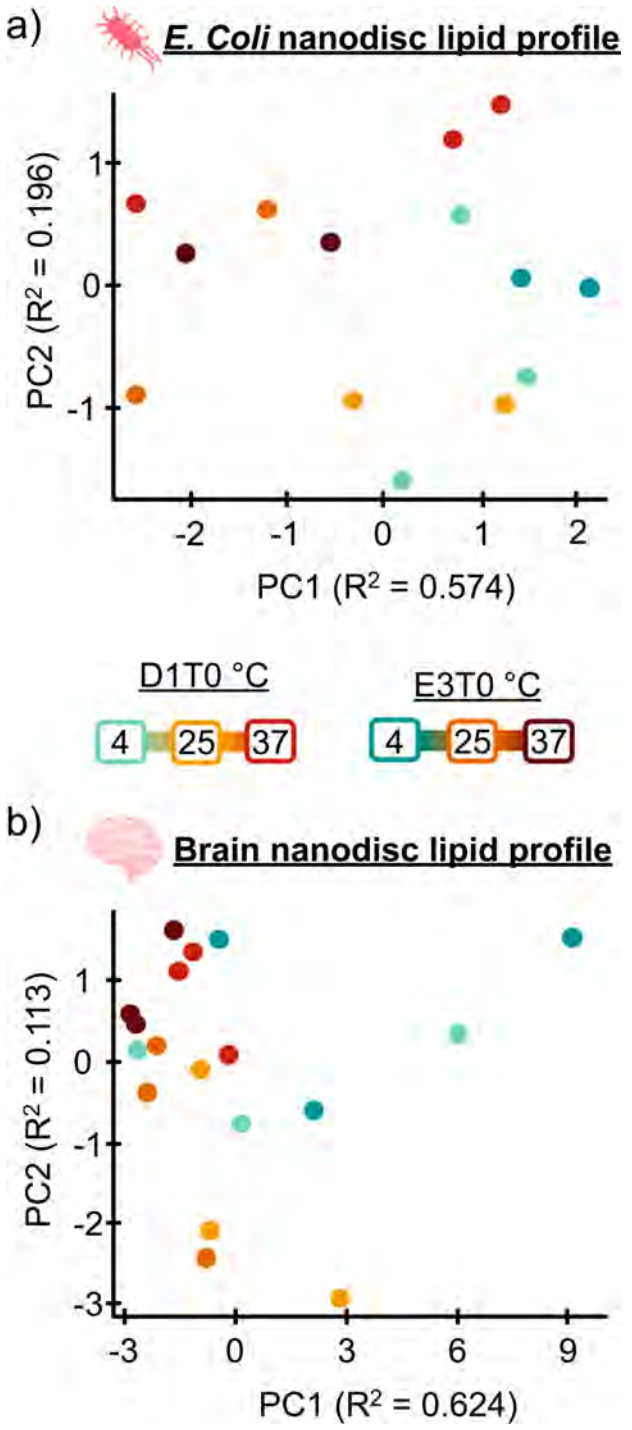

Figure 1. Global lipid profiles across nanodisc assembly conditions. (a) Principal component analysis (PCA) of replicate nanodisc assembly global lipid differences for *E. coli* polar lipid extract. (b) PCA of nanodisc assembly global lipid differences for porcine brain polar lipid extract. Dot colors match the annotated belt and assembly conditions between the plots.

discovered strong conservation of lipid profiles within *E. coli* nanodiscs of different sizes.

Effects of Assembly Temperature. As described above, lipid packing in nanodiscs is affected by assembly temperature, which can be an important parameter to tune in order to optimize assembly.[57,58] Therefore, we tested for lipid uptake biases across three assembly temperatures for both the smaller and larger nanodisc sizes (Figure 2B). Both sizes were compared between assembly at cold (4 °C), room (25 °C), and physiological temperatures (37 °C). In our initial assessment of individual lipid changes within smaller D1 nanodiscs, only 2 (4%) out of 55 identified lipids were differentially incorporated at higher temperatures, suggesting very limited effects of assembly temperature on the individual lipid profiles.

With the larger E3 comparisons, the number of significant lipids increased to 11 (20% of identified lipids), with 2 PEs, 4 CLs, and 5 PGs. To further explore the trends to lipid perturbations in the E3 nanodiscs, we compared the relative area changes of significant lipids across each temperature (Figure 2C). Here, a trend of the individual lipids emerged where all significant CLs (25% of total CLs) were more abundant at 4 °C and all significant PG lipids (31% of total PGs) were elevated at 25 and 37 °C.

To test whether these trends in individual lipids were reflected in the class broadly, the total mole percent of the three lipid classes were calculated using internal standards. Here, the ratios in the classes when comparing E3 nanodiscs between 4 and 37 °C confirmed the general trend of enrichment for CL at lower temperature (from 13 to 8 mol %, $p = 0.003$) and for PG at higher temperature (from 23 to 33 mol %, $p = 0.15$) (Table S5, Figure 3). Although the trend was not statistically significant on a class level for PG between 4 and 37 °C, the comparison of 4 and 25 °C was significant for the PG class ($p = 0.003$).

Because the MSP:lipid ratio used during assembly and nanodisc sizes are constant for all assembly temperatures, the area per lipid should increase in warmer conditions. For CLs, the colder assembly temperature provides a smaller mean surface area per lipid that better accommodates these bulkier lipids, which are twice the size of other phospholipids. This effect may be more prominent in E3 than D1 because the ∼2-fold increase in lipid surface area for E3 nanodiscs may give the bilayer more room to expand and contract. Conversely, some PG and PE lipids increased in the more crowded 25 and 37 °C nanodiscs, where they were preferred over the bulkier CLs. No clear fatty acid properties distinguish the significant lipids in these classes from the library of all lipids identified with our analytical method.

Collectively, the incorporation of *E. coli* polar lipids from a natural extract showed globally conserved lipid content. This consistency largely agreed with applications of SMALPs assembled from isolated lipid membranes.[31] However, certain structural groups seem to contain some subtle fluctuations to favor bulkier lipids in cold conditions with larger nanodiscs. Understanding these effects is important for establishing a baseline for future applications of nanodiscs with heterogeneous lipid extracts.

Nanodisc Assembly from Brain Polar Lipid Extract. Unlike bacterial lipids, mammalian lipids offer a significant diversity in lipid category and class that provides a broad range of physiochemical characteristics. This biological diversity may exacerbate biases in assembly of nanodiscs that model mammalian membranes. To test how lipid profiles were affected, we assembled nanodiscs with porcine brain lipid extract under the same range of conditions.

We developed and validated our lipidomic library using the brain lipid extract and LC-DDA data with manual inspection and quality control cutoffs. We confidently annotated 279 lipids across three categories: sphingolipids (35), glycerophos-

https://doi.org/10.1021/jasms.3c00170
J. Am. Soc. Mass Spectrom. 2023, 34, 2006−2015

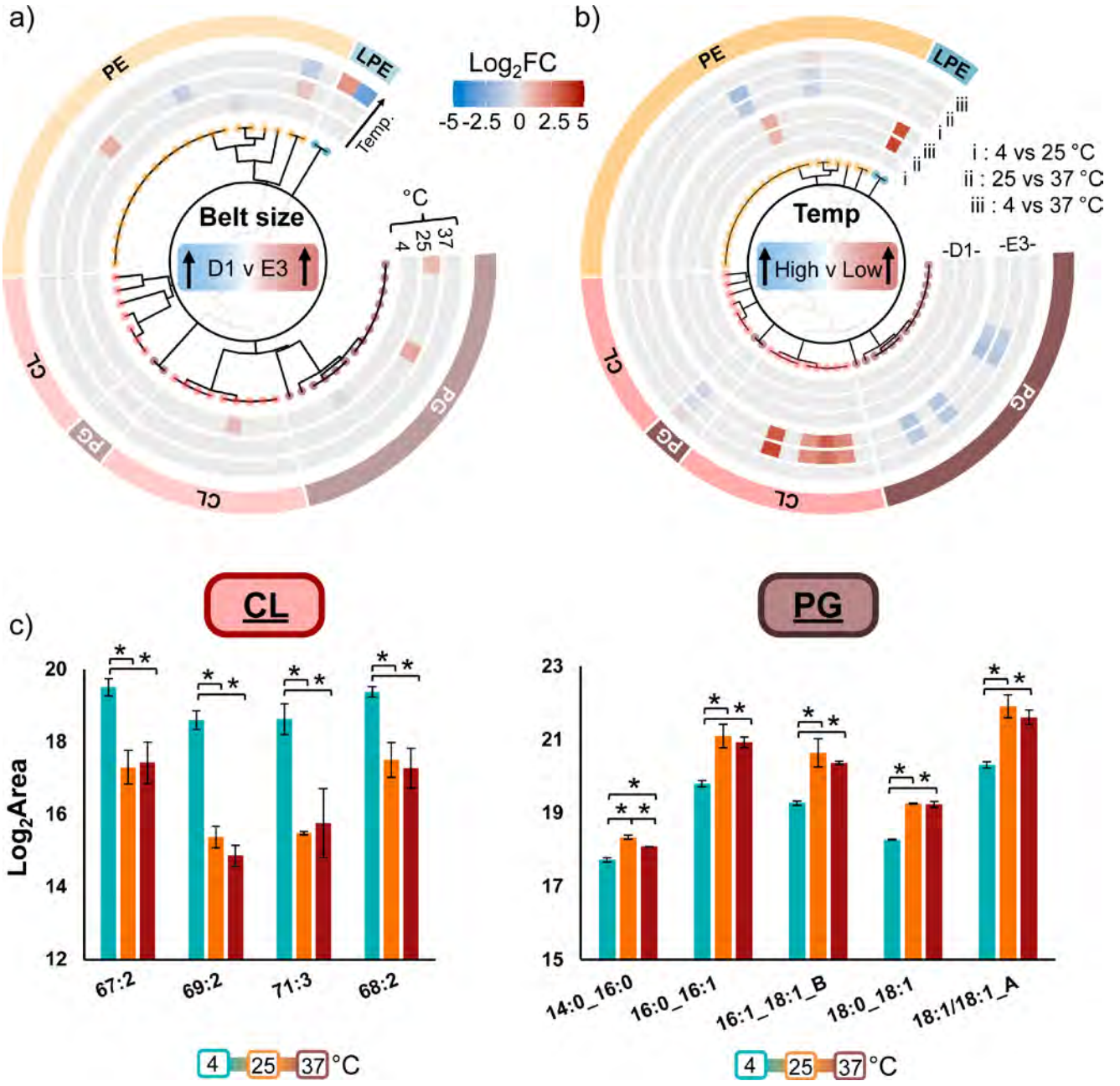

Figure 2. *E. coli* lipid uptake across nanodisc assembly conditions. (a) Circular dendrogram of all 55 lipids identified in *E. coli* and their differential expression in D1 vs E3 nanodiscs at various assembly temperatures, shown as different ring levels. (b) Circular dendrogram of lipid uptake differences at 4 vs 25 °C (inner ring), 25 vs 37 °C (middle ring), and 4 vs 37 °C (outer ring) for E3 and D1 nanodiscs. Separation of PG and CL classes in dendrograms reflects fatty acyl saturation vs unsaturation differences. Fold change heatmaps are normalized to the greatest fold change differences across both (a) and (b) comparisons. (c) Abundance profiles of significant lipids across temperature comparisons with E3 nanodiscs of select cardiolipin (CL, left) and phosphatidylglycerol (PG, right) lipids. Fatty acyl compositions for each lipid are annotated below with either sum composition for the CL or individual composition for PG. Significant differences between downward ticks on the lines are marked with an *.

pholipids (220), and glycerolipids (24) (Figure 4A). From these lipids, 12 classes were observed with the greatest coverage for abundant phospholipid classes, especially phosphatidylcholine (PC) and PE, triglycerides (TG), and hexosyl-ceramides (HexCer) lipid classes. Fatty acyl coverage across the 279 lipids identified here also showed coverage of various chain lengths and unsaturation, with polyunsaturated (PUFA) and monounsaturated (MUFA) tails being most abundant (Figure 4A). Notably, although the total number of identifications between lipid studies is often variable due to challenges separating isomeric species and differences in the lipid speciation levels achievable across analytical platforms, the overall profile of lipid class coverage observed in this method agreed with prior lipidomic analyses of mammalian systems.[45,46]

Effects of Nanodisc Size. As with *E. coli* lipid extracts, we measured the effect of MSP belt size on brain lipid uptake at three temperatures of incubation. Of the 279 identified lipids, we observed a total of 55 (20%, 20 lipids at greater levels in D1, 35 lipids greater in E3) significant differences in lipid uptake between the D1 versus E3 MSP diameters at one or

https://doi.org/10.1021/jasms.3c00170
J. Am. Soc. Mass Spectrom. 2023, 34, 2006−2015

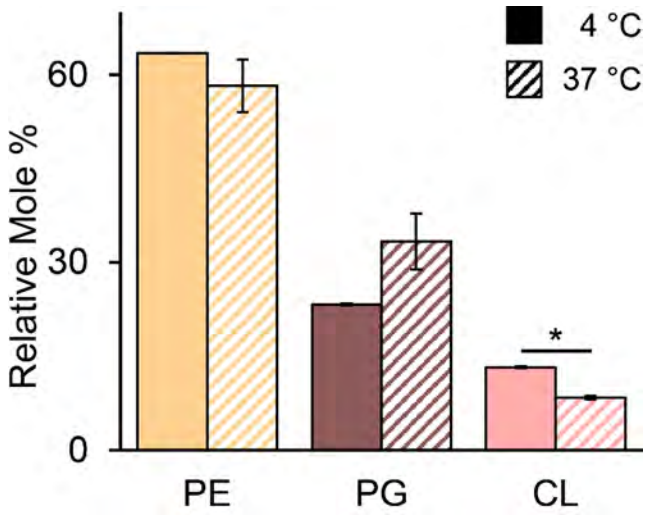

Figure 3. Relative mole percentage of PE, PG, and CL lipids in E3 nanodiscs assembled at 4 (solid) and 37 °C (dashed). Statistical comparisons are provided in Table S5, and significant differences ($p < 0.05$) are marked with an *.

more temperatures, which suggest nanodisc size impacts lipid uptake.

Examining each assembly temperature, we observed an increasing number of significant lipid fluctuations at higher temperatures (Figure 4B). At 4 °C, only 5 lipids (3 elevated in E3 and 2 elevated in D1) were differentially incorporated in the different belt diameters. At 25 °C, 8 lipids changed significantly (2 elevated in E3 and 6 elevated in D1), and 37 °C included 44 significant lipid changes (16 at greater levels in E3 and 28 at greater levels in D1).

To identify structural motifs with clear relationships to the belt diameter, we tested for enrichment of significant lipid profiles relative to our brain lipid library (Figure 4C).[50] No clear trends were seen at 4 °C due to the relatively minimal changes. Of the 8 significantly changing lipids at 25 °C, 4 were sphingolipids, 3 HexCer and 1 ceramide (Cer), that were integrated at lower levels in E3 compared to their D1 counterparts. These changes drove significant sphingolipid category enrichment. Nanodiscs assembled at 37 °C had the most significant differences in lipid uptake between different diameters. Of the 44 significantly altered lipids, HexCer (15 increasing in D1) and phosphatidyl-inositol (PI, 4 increasing in E3) lipid classes were significantly enriched structural classes. Although both lipids include a bulky sugar moiety, we observed that the trends to preferential uptake diverged, with PI favored in E3 and HexCer favored in D1.

Comparing changes in the relative class composition gave similar results (Figure 5), with HexCer lipids significantly decreasing in E3 nanodiscs at 25 and 37 °C. PI lipids increased in larger E3 nanodiscs but with weak statistical significance. Although no individual lipids changed significantly, the sphingomyelin (SM) lipids decreased significantly in E3 at 25 and 37 °C. No significant class changes were observed at 4 °C, which demonstrates that these class differences between nanodiscs of different sizes primarily occur at higher assembly temperatures. No major statistically significant changes were observed in the average lipid tail lengths or unsaturation for any classes.

One potential explanation for our observations could be related to differences in hydrogen bonding. PI lipids have an average of around 1 hydrogen bond to other phospholipids.[59] Conversely, galactose-ceramide (GalCer) lipids, the predominant form of HexCer in brain tissue, can have an average of 2 hydrogen bonds.[60,61] To facilitate the multiple bonds of GalCer lipids, it has been suggested that GalCer presence at 5−10 mol % results in a unique lipid organization where GalCer lipids nestle slightly below other phospholipids.[60,62] We hypothesize that these interactions may be more favored at the edge of the nanodiscs, which represent a greater fraction of the lipids in D1 nanodiscs than the larger E3 nanodiscs. However, it could be that other differences in the glycerophospholipid versus sphingolipid backbone could affect incorporation, which could explain SM decreasing in larger nanodiscs at higher temperatures.

Effects of Assembly Temperature. Following our analysis of lipid uptake differences across various nanodisc diameters, we next sought to understand how temperature could serve as a primary modulator of lipid uptake. From our comparison of lipid abundances across 279 lipids, a total of 9 unique lipids (3%) were significantly influenced by temperature for D1 nanodiscs (Figure 4D). These differences included 2 significant lipids at 4 versus 25 °C, 8 significant lipids at 25 versus 37 °C, and 3 significant lipids at 4 versus 37 °C. Clearly, there were very limited effects of assembly temperature on lipid profiles of D1 nanodiscs. In the total class analysis, there were small but significant changes in CL, but no major changes were significant in the relative class composition.

Conversely, the E3 nanodiscs included 20 significant lipid fluctuations (7%) at various temperatures, with 15 significant lipids at 4 versus 25 °C, 1 significant lipid at 25 versus 37 °C, and 14 significant lipids at 4 versus 37 °C. There were no clear trends within or between the D1 and E3 comparisons, suggesting that there are not strong biases in incorporation caused by assembly temperature. With the relative class composition, some similar trends were observed to the changes in nanodisc size, with significant increases in PI at higher temperatures in E3 nanodiscs, but these were only significant when comparing 4 to 37 °C.

We again completed an enrichment analysis by comparing all lipid fluctuations related to temperature for a single belt size (Figure 4E). For the total of 13 unique, significant lipid identifications in the D1 belt, we observed three cardiolipins that were significantly enriched. Notably, the trend to cardiolipin agreed with the *E. coli* polar lipid extract, with CL elevated at lower temperatures. Conversely, other lipid classes were not significantly enriched in the changing lipids. Thus, there were limited trends in the effect of assembly temperature on brain lipid uptake.

Initially, we anticipated that fluctuations in lipid uptake would likely reflect phase transition temperature, a physiochemical property that differentiates the ordering of lipids into gel and liquid phases that is primarily driven by fatty acyl composition.[63] However, our observation of differential lipid uptake within different MSP belts suggests that individual lipid phase transition temperature is not a predominant factor in the differential uptake of natural lipids from complex extracts into nanodiscs. Instead, our analysis suggests that lipid uptake is more complex and influenced by the lipid environment that depends on assembly temperature and nanodisc size.

We also note that cholesterol, a key modulator of lipid assembly in mammalian models, is undetected in this study due to its poor ionization (shown in the Supporting Information). Cholesterol makes up approximately 30% of

https://doi.org/10.1021/jasms.3c00170
J. Am. Soc. Mass Spectrom. 2023, 34, 2006−2015

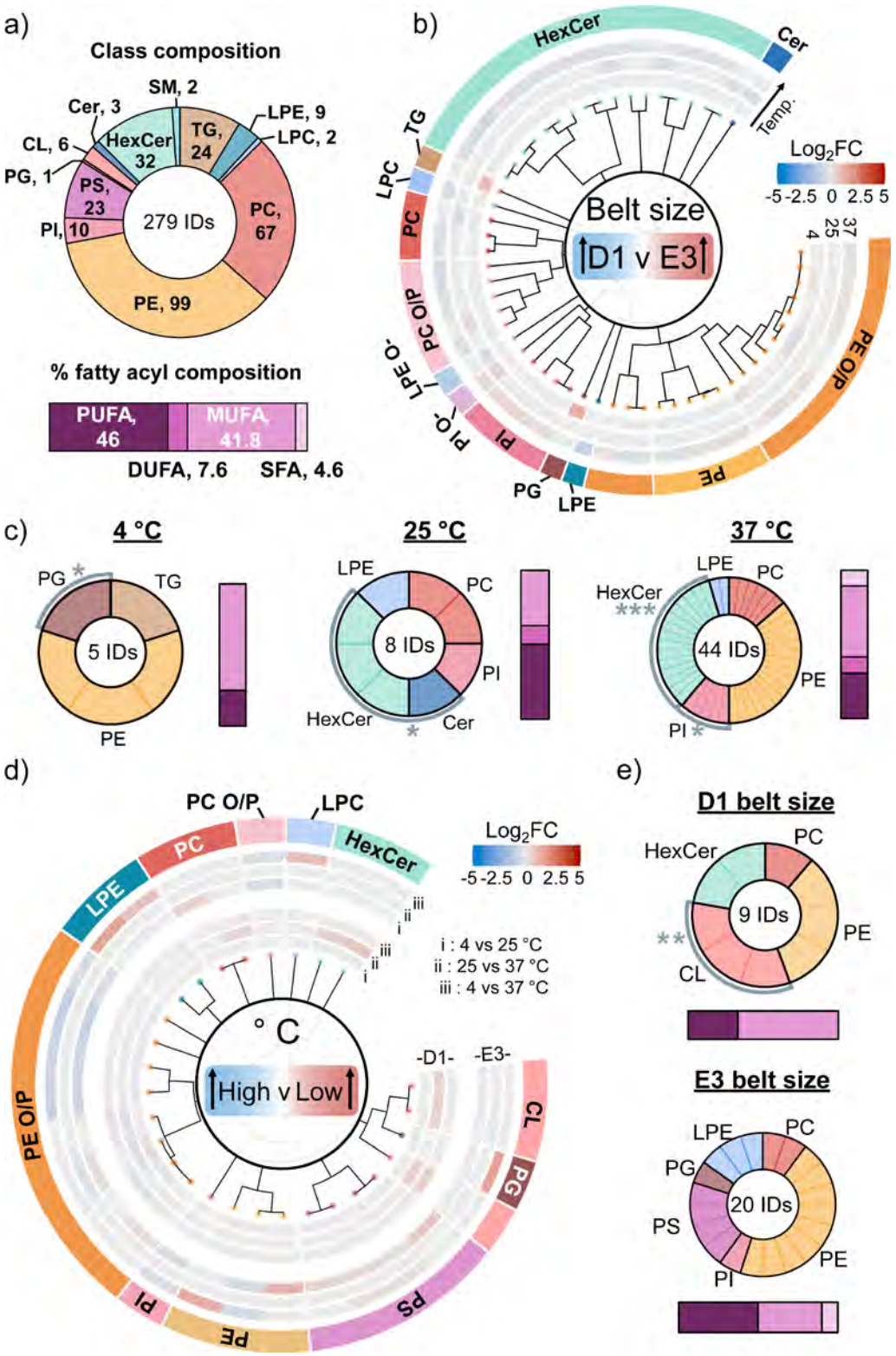

Figure 4. Porcine polar brain lipid uptake across nanodisc assembly conditions. (a) Lipid class and fatty acyl profiles for the brain lipid library. (b) Circular dendrogram of the significant lipid changes across E3 vs D1 comparisons. (c) Enrichment analysis output for all significant lipids in E3 vs D1 comparisons at 4 °C (left), 25 °C (middle), and 37 °C (right). (d) Circular dendrogram of significant lipids across temperature effects. (e) Enrichment analysis output for all significant lipids within D1 (top) and E3 (bottom). All dendrograms were coded with the same heatmap to relate significant lipid changes across each biological lipid extract and assembly condition comparison. Significantly enriched motifs in c and e are noted with stars corresponding to *p*-values (* < 0.05, ** < 0.005, *** < 0.0005).

the lipid bilayer and has modulatory effects on the surrounding lipids due to its rigidity.[64,65] For example, at relatively low levels cholesterol assembles neighboring lipids into an ordered phase, making it a key regulator of lipid phase behavior.[66,67] At

https://doi.org/10.1021/jasms.3c00170
J. Am. Soc. Mass Spectrom. 2023, 34, 2006−2015

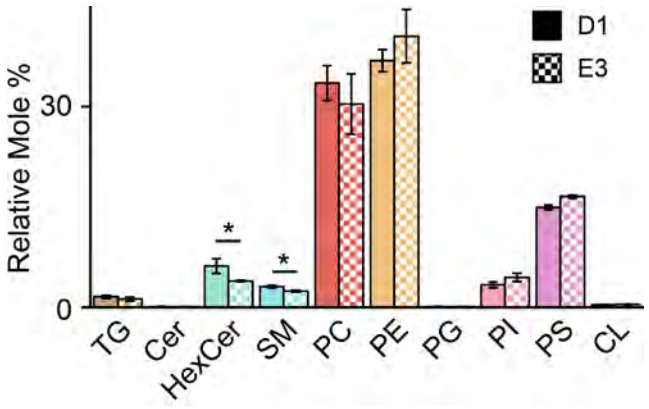

Figure 5. Relative mole percentage of brain polar lipid extract classes in nanodiscs assembled at 37 °C with either D1 (solid) or E3 (dashed) belts. Statistical comparisons are provided in Table S5, and significant differences (adjusted $p < 0.1$) are marked with an *.

this phase, the cholesterol will help straighten the fatty acyl chains of lipids while also promoting the lateral diffusion of the lipids.[68] Therefore, differential cholesterol uptake may also play a role in our observations, but we are unable to detect it with our current lipidomic method.

CONCLUSIONS

Nanodiscs are a promising technology for solubilizing membrane proteins in bilayers formed from natural lipid extracts that mimic biological membranes. However, the diversity of biological lipids makes this integration nontrivial, and it is important to investigate potential bias of lipid species in nanodisc assembly. A first step toward understanding the robustness of natural lipid nanodiscs is understanding how nanodisc profiles vary across assembly factors. In our analysis of natural lipid extract incorporation of both bacterial and mammalian lipids, we discovered that global lipid profiles were largely unchanged, indicating that nanodiscs can robustly incorporate natural lipids across a range of assembly conditions.

However, a few subtle lipid changes were seen across both nanodisc size and assembly temperature. From our analysis of the *E. coli* polar lipid extract, we observed a greater effect on lipid uptake from assembly temperature compared to nanodisc size. In contrast, brain polar lipid extract showed greater fluctuations with nanodisc size, particularly at higher temperatures. In general, nanodisc lipid profiles were most consistent for smaller nanodiscs assembled at colder temperatures, with greater variations in larger nanodiscs at higher temperatures. Thus, assembly of smaller nanodiscs or at colder temperatures is recommended for consistent lipidome incorporation. However, additional studies will be needed to explore additional types of lipid mixtures, additional MSP belts, and to compare the lipidomic profile of the nanodiscs with the starting lipid extract dissolved in either detergents or organic solvents.

From these findings, we were able to first show how lipid fluctuations, although present, are largely marginal. Additionally, we also showed several trends to lipid fluctuations that we can relate to structural features like lipid size, thereby better understanding how differences in nanodisc assembly may influence lipid uptake. Altogether, our study is a key starting point for the expansion of nanodiscs to incorporate more native lipid environments.

ASSOCIATED CONTENT

Data Availability Statement

All raw data for this manuscript is available at MassIVE (DOI: 10.25345/C5G737D8J, MSV000091857)

Supporting Information

The Supporting Information is available free of charge at https://pubs.acs.org/doi/10.1021/jasms.3c00170.

Tables S1−S5 with LC gradient conditions, full results, and statistics (XLSX)

AUTHOR INFORMATION

Corresponding Author

Michael T. Marty − *Department of Chemistry and Biochemistry, University of Arizona, Tucson, AZ 85721, United States; BioS Institute, University of Arizona, Tucson, AZ 85721, United States;* orcid.org/0000-0001-8115-1772; Email: mtmarty@arizona.edu

Authors

Melanie T. Odenkirk − *Department of Chemistry and Biochemistry, University of Arizona, Tucson, AZ 85721, United States; BioS Institute, University of Arizona, Tucson, AZ 85721, United States*

Guozhi Zhang − *Department of Chemistry and Biochemistry, University of Arizona, Tucson, AZ 85721, United States*

Complete contact information is available at: https://pubs.acs.org/10.1021/jasms.3c00170

Author Contributions

M.T.O. and G.Z. contributed equally to this work.

Notes

The authors declare no competing financial interest.

ACKNOWLEDGMENTS

The authors would like to acknowledge NIH/NIGMS Grant R35 GM128624 for funding. The authors thank Prof. Stephen Sligar for the MSP plasmids (Addgene #20061) and (Addgene #20066).

REFERENCES

(1) Liebisch, G.; Fahy, E.; Aoki, J.; Dennis, E. A.; Durand, T.; Ejsing, C. S.; Fedorova, M.; Feussner, I.; Griffiths, W. J.; Köfeler, H.; Merrill, A. H.; Murphy, R. C.; O'Donnell, V. B.; Oskolkova, O.; Subramaniam, S.; Wakelam, M. J. O.; Spener, F. Update on LIPID MAPS classification, nomenclature, and shorthand notation for MS-derived lipid structures. *J. Lipid Res.* **2020**, *61* (12), 1539−1555.

(2) Sohlenkamp, C.; Geiger, O. Bacterial membrane lipids: diversity in structures and pathways. *FEMS Microbiol Rev.* **2016**, *40* (1), 133−59.

(3) Mileykovskaya, E.; Dowhan, W. Cardiolipin membrane domains in prokaryotes and eukaryotes. *Biochim. Biophys. Acta* **2009**, *1788* (10), 2084−91.

(4) Pluhackova, K.; Horner, A. Native-like membrane models of E. coli polar lipid extract shed light on the importance of lipid composition complexity. *BMC biology* **2021**, *19* (1), 4.

(5) Mileykovskaya, E.; Dowhan, W. Role of membrane lipids in bacterial division-site selection. *Curr. Opin Microbiol* **2005**, *8* (2), 135−42.

(6) Zheng, C.; Han, L.; Yap, C. W.; Xie, B.; Chen, Y. Progress and problems in the exploration of therapeutic targets. *Drug Discov Today* **2006**, *11* (9−10), 412−20.
(7) Cournia, Z.; Allen, T. W.; Andricioaei, I.; Antonny, B.; Baum, D.; Brannigan, G.; Buchete, N. V.; Deckman, J. T.; Delemotte, L.; Del Val, C.; Friedman, R.; Gkeka, P.; Hege, H. C.; Hénin, J.; Kasimova, M. A.; Kolocouris, A.; Klein, M. L.; Khalid, S.; Lemieux, M. J.; Lindow, N.; Roy, M.; Selent, J.; Tarek, M.; Tofoleanu, F.; Vanni, S.; Urban, S.; Wales, D. J.; Smith, J. C.; Bondar, A. N. Membrane Protein Structure, Function, and Dynamics: a Perspective from Experiments and Theory. *J. Membr. Biol.* **2015**, *248* (4), 611−40.
(8) Laganowsky, A.; Reading, E.; Allison, T. M.; Ulmschneider, M. B.; Degiacomi, M. T.; Baldwin, A. J.; Robinson, C. V. Membrane proteins bind lipids selectively to modulate their structure and function. *Nature* **2014**, *510* (7503), 172−175.
(9) Sezgin, E.; Azbazdar, Y.; Ng, X. W.; Teh, C.; Simons, K.; Weidinger, G.; Wohland, T.; Eggeling, C.; Ozhan, G. Binding of canonical Wnt ligands to their receptor complexes occurs in ordered plasma membrane environments. *FEBS J.* **2017**, *284* (15), 2513−2526.
(10) Zwaal, R. F.; Comfurius, P.; Bevers, E. M. Lipid-protein interactions in blood coagulation. *Biochim. Biophys. Acta* **1998**, *1376* (3), 433−53.
(11) Stace, C. L.; Ktistakis, N. T. Phosphatidic acid- and phosphatidylserine-binding proteins. *Biochim. Biophys. Acta* **2006**, *1761* (8), 913−26.
(12) Denisov, I. G.; Sligar, S. G. Nanodiscs in Membrane Biochemistry and Biophysics. *Chem. Rev.* **2017**, *117* (6), 4669−4713.
(13) Früh, V.; Zhou, Y.; Chen, D.; Loch, C.; Ab, E.; Grinkova, Y. N.; Verheij, H.; Sligar, S. G.; Bushweller, J. H.; Siegal, G. Application of fragment-based drug discovery to membrane proteins: identification of ligands of the integral membrane enzyme DsbB. *Chem. Biol.* **2010**, *17* (8), 881−91.
(14) Gardill, B.; Huang, J.; Tu, L.; Van Petegem, F.; Oxenoid, K.; Thomson, C. A. Nanodisc technology facilitates identification of monoclonal antibodies targeting multi-pass membrane proteins. *Sci. Rep* **2020**, *10* (1), 1130.
(15) Broecker, J.; Eger, B. T.; Ernst, O. P. Crystallogenesis of Membrane Proteins Mediated by Polymer-Bounded Lipid Nanodiscs. *Structure* **2017**, *25* (2), 384−392.
(16) Efremov, R. G.; Gatsogiannis, C.; Raunser, S. Lipid Nanodiscs as a Tool for High-Resolution Structure Determination of Membrane Proteins by Single-Particle Cryo-EM. *Methods Enzymol* **2017**, *594*, 1−30.
(17) Hagn, F.; Nasr, M. L.; Wagner, G. Assembly of phospholipid nanodiscs of controlled size for structural studies of membrane proteins by NMR. *Nat. Protoc* **2018**, *13* (1), 79−98.
(18) Kostelic, M. M.; Zak, C. K.; Jayasekera, H. S.; Marty, M. T. Assembly of Model Membrane Nanodiscs for Native Mass Spectrometry. *Anal. Chem.* **2021**, *93* (14), 5972−5979.
(19) Panda, A.; Giska, F.; Duncan, A. L.; Welch, A. J.; Brown, C.; McAllister, R.; Hariharan, P.; Goder, J. N. D.; Coleman, J.; Ramakrishnan, S.; Pincet, F.; Guan, L.; Krishnakumar, S.; Rothman, J. E.; Gupta, K. Direct determination of oligomeric organization of integral membrane proteins and lipids from intact customizable bilayer. *Nat. Methods* **2023**, *20* (6), 891−897.
(20) Denisov, I. G.; Sligar, S. G. Nanodiscs for structural and functional studies of membrane proteins. *Nature structural & molecular biology* **2016**, *23* (6), 481−486.
(21) Civjan, N. R.; Bayburt, T. H.; Schuler, M. A.; Sligar, S. G. Direct solubilization of heterologously expressed membrane proteins by incorporation into nanoscale lipid bilayers. *BioTechniques* **2003**, *35* (3), 556−60.
(22) Reid, D. J.; Rohrbough, J. G.; Kostelic, M. M.; Marty, M. T. Investigating Antimicrobial Peptide-Membrane Interactions Using Fast Photochemical Oxidation of Peptides in Nanodiscs. *J. Am. Soc. Mass Spectrom.* **2022**, *33* (1), 62−67.
(23) Kostelic, M. M.; Zak, C. K.; Liu, Y.; Chen, V. S.; Wu, Z.; Sivinski, J.; Chapman, E.; Marty, M. T. UniDecCD: Deconvolution of Charge Detection-Mass Spectrometry Data. *Anal. Chem.* **2021**, *93* (44), 14722−14729.
(24) Gao, Y.; Cao, E.; Julius, D.; Cheng, Y. TRPV1 structures in nanodiscs reveal mechanisms of ligand and lipid action. *Nature* **2016**, *534* (7607), 347−51.
(25) Frauenfeld, J.; Gumbart, J.; Sluis, E. O.; Funes, S.; Gartmann, M.; Beatrix, B.; Mielke, T.; Berninghausen, O.; Becker, T.; Schulten, K.; Beckmann, R. Cryo-EM structure of the ribosome-SecYE complex in the membrane environment. *Nat. Struct Mol. Biol.* **2011**, *18* (5), 614−21.
(26) Rues, R. B.; Dötsch, V.; Bernhard, F. Co-translational formation and pharmacological characterization of beta1-adrenergic receptor/nanodisc complexes with different lipid environments. *Biochim. Biophys. Acta* **2016**, *1858* (6), 1306−16.
(27) Yusuf, Y.; Massiot, J.; Chang, Y. T.; Wu, P. H.; Yeh, V.; Kuo, P. C.; Shiue, J.; Yu, T. Y. Optimization of the Production of Covalently Circularized Nanodiscs and Their Characterization in Physiological Conditions. *Langmuir* **2018**, *34* (11), 3525−3532.
(28) Dijkman, P. M.; Watts, A. Lipid modulation of early G protein-coupled receptor signalling events. *Biochim. Biophys. Acta* **2015**, *1848* (11), 2889−97.
(29) Lee, S. C.; Knowles, T. J.; Postis, V. L.; Jamshad, M.; Parslow, R. A.; Lin, Y. P.; Goldman, A.; Sridhar, P.; Overduin, M.; Muench, S. P.; Dafforn, T. R. A method for detergent-free isolation of membrane proteins in their local lipid environment. *Nat. Protoc* **2016**, *11* (7), 1149−62.
(30) Dörr, J. M.; Scheidelaar, S.; Koorengevel, M. C.; Dominguez, J. J.; Schäfer, M.; van Walree, C. A.; Killian, J. A. The styrene-maleic acid copolymer: a versatile tool in membrane research. *Eur. Biophys J.* **2016**, *45* (1), 3−21.
(31) Teo, A. C. K.; Lee, S. C.; Pollock, N. L.; Stroud, Z.; Hall, S.; Thakker, A.; Pitt, A. R.; Dafforn, T. R.; Spickett, C. M.; Roper, D. I. Analysis of SMALP co-extracted phospholipids shows distinct membrane environments for three classes of bacterial membrane protein. *Sci. Rep* **2019**, *9* (1), 1813.
(32) van 't Klooster, J. S.; Cheng, T. Y.; Sikkema, H. R.; Jeucken, A.; Moody, B.; Poolman, B. Periprotein lipidomes of Saccharomyces cerevisiae provide a flexible environment for conformational changes of membrane proteins. *Elife* **2020**, *9*, No. e57003.
(33) Barniol-Xicota, M.; Verhelst, S. H. L. Lipidomic and in-gel analysis of maleic acid co-polymer nanodiscs reveals differences in composition of solubilized membranes. *Commun. Biol.* **2021**, *4* (1), 218.
(34) Li, M. J.; Atkins, W. M.; McClary, W. D. Preparation of Lipid Nanodiscs with Lipid Mixtures. *Curr. Protoc Protein Sci.* **2019**, *98* (1), No. e100.
(35) Denisov, I. G.; Grinkova, Y. V.; Lazarides, A. A.; Sligar, S. G. Directed self-assembly of monodisperse phospholipid bilayer Nanodiscs with controlled size. *J. Am. Chem. Soc.* **2004**, *126* (11), 3477−87.
(36) Reid, D. J.; Diesing, J. M.; Miller, M. A.; Perry, S. M.; Wales, J. A.; Montfort, W. R.; Marty, M. T. MetaUniDec: High-Throughput Deconvolution of Native Mass Spectra. *J. Am. Soc. Mass Spectrom.* **2019**, *30* (1), 118−127.
(37) Reid, D. J.; Keener, J. E.; Wheeler, A. P.; Zambrano, D. E.; Diesing, J. M.; Reinhardt-Szyba, M.; Makarov, A.; Marty, M. T. Engineering Nanodisc Scaffold Proteins for Native Mass Spectrometry. *Anal. Chem.* **2017**, *89* (21), 11189−11192.
(38) Marty, M. T.; Hoi, K. K.; Gault, J.; Robinson, C. V. Probing the Lipid Annular Belt by Gas-Phase Dissociation of Membrane Proteins in Nanodiscs. *Angewandte Chemie (International ed. in English)* **2016**, *55* (2), 550−4.
(39) Freeman, C.; Hynds, H. M.; Carpenter, J. M.; Appala, K.; Bimpeh, K.; Barbarek, S.; Gatto, C.; Wilkinson, B. J.; Hines, K. M. Revealing Fatty Acid Heterogeneity in Staphylococcal Lipids with Isotope Labeling and RPLC-IM-MS. *J. Am. Soc. Mass Spectrom.* **2021**, *32* (9), 2376−2385.
(40) Pasa-Tolić, L.; Masselon, C.; Barry, R. C.; Shen, Y.; Smith, R. D. Proteomic analyses using an accurate mass and time tag strategy. *Biotechniques* **2004**, *37* (4), 621−4.

https://doi.org/10.1021/jasms.3c00170
J. Am. Soc. Mass Spectrom. 2023, 34, 2006−2015

(41) Tsugawa, H.; Cajka, T.; Kind, T.; Ma, Y.; Higgins, B.; Ikeda, K.; Kanazawa, M.; VanderGheynst, J.; Fiehn, O.; Arita, M. MS-DIAL: data-independent MS/MS deconvolution for comprehensive metabolome analysis. *Nat. Methods* **2015**, *12* (6), 523−6.
(42) Tsugawa, H.; Ikeda, K.; Takahashi, M.; Satoh, A.; Mori, Y.; Uchino, H.; Okahashi, N.; Yamada, Y.; Tada, I.; Bonini, P.; Higashi, Y.; Okazaki, Y.; Zhou, Z.; Zhu, Z.-J.; Koelmel, J.; Cajka, T.; Fiehn, O.; Saito, K.; Arita, M.; Arita, M. A lipidome atlas in MS-DIAL 4. *Nat. Biotechnol.* **2020**, *38* (10), 1159−1163.
(43) Hines, K. M.; Xu, L. Lipidomic consequences of phospholipid synthesis defects in Escherichia coli revealed by HILIC-ion mobility-mass spectrometry. *Chem. Phys. Lipids* **2019**, *219*, 15−22.
(44) Kralj, T.; Nuske, M.; Hofferek, V.; Sani, M. A.; Lee, T. H.; Separovic, F.; Aguilar, M. I.; Reid, G. E. Multi-Omic Analysis to Characterize Metabolic Adaptation of the. *Metabolites* **2022**, *12* (2), 171.
(45) Fitzner, D.; Bader, J. M.; Penkert, H.; Bergner, C. G.; Su, M.; Weil, M. T.; Surma, M. A.; Mann, M.; Klose, C.; Simons, M. Cell-Type- and Brain-Region-Resolved Mouse Brain Lipidome. *Cell Rep* **2020**, *32* (11), 108132.
(46) Quehenberger, O.; Armando, A. M.; Brown, A. H.; Milne, S. B.; Myers, D. S.; Merrill, A. H.; Bandyopadhyay, S.; Jones, K. N.; Kelly, S.; Shaner, R. L.; Sullards, C. M.; Wang, E.; Murphy, R. C.; Barkley, R. M.; Leiker, T. J.; Raetz, C. R.; Guan, Z.; Laird, G. M.; Six, D. A.; Russell, D. W.; McDonald, J. G.; Subramaniam, S.; Fahy, E.; Dennis, E. A. Lipidomics reveals a remarkable diversity of lipids in human plasma. *J. Lipid Res.* **2010**, *51* (11), 3299−305.
(47) Adams, K. J.; Pratt, B.; Bose, N.; Dubois, L. G.; St. John-Williams, L.; Perrott, K. M.; Ky, K.; Kapahi, P.; Sharma, V.; MacCoss, M. J.; Moseley, M. A.; Colton, C. A.; MacLean, B. X.; Schilling, B.; Thompson, J. W. Skyline for Small Molecules: A Unifying Software Package for Quantitative Metabolomics. *J. Proteome Res.* **2020**, *19* (4), 1447−1458.
(48) Stratton, K. G.; Webb-Robertson, B. M.; McCue, L. A.; Stanfill, B.; Claborne, D.; Godinez, I.; Johansen, T.; Thompson, A. M.; Burnum-Johnson, K. E.; Waters, K. M.; Bramer, L. M. pmartR: Quality Control and Statistics for Mass Spectrometry-Based Biological Data. *J. Proteome Res.* **2019**, *18* (3), 1418−1425.
(49) Wei, R.; Wang, J.; Su, M.; Jia, E.; Chen, S.; Chen, T.; Ni, Y. Missing Value Imputation Approach for Mass Spectrometry-based Metabolomics Data. *Sci. Rep* **2018**, *8* (1), 663.
(50) Clair, G.; Reehl, S.; Stratton, K. G.; Monroe, M. E.; Tfaily, M. M.; Ansong, C.; Kyle, J. E. Lipid Mini-On: mining and ontology tool for enrichment analysis of lipidomic data. *Bioinformatics* **2019**, *35* (21), 4507−4508.
(51) Odenkirk, M. T.; Zin, P. P. K.; Ash, J. R.; Reif, D. M.; Fourches, D.; Baker, E. S. Structural-based connectivity and omic phenotype evaluations (SCOPE): a cheminformatics toolbox for investigating lipidomic changes in complex systems. *Analyst* **2020**, *145* (22), 7197−7209.
(52) Schachter, I.; Harries, D. Capturing Lipid Nanodisc Shape and Properties Using a Continuum Elastic Theory. *J. Chem. Theory Comput* **2023**, *19* (4), 1360−1369.
(53) Schachter, I.; Allolio, C.; Khelashvili, G.; Harries, D. Confinement in Nanodiscs Anisotropically Modifies Lipid Bilayer Elastic Properties. *J. Phys. Chem. B* **2020**, *124* (33), 7166−7175.
(54) Real Hernandez, L. M.; Levental, I. Lipid packing is disrupted in copolymeric nanodiscs compared with intact membranes. *Biophys. J.* **2023**, *122* (11), 2256−2266.
(55) Silvius, J. R. Fluorescence Energy Transfer Reveals Microdomain Formation at Physiological Temperatures in Lipid Mixtures Modeling the Outer Leaflet of the Plasma Membrane. *Biophys. J.* **2003**, *85* (2), 1034−1045.
(56) Høyrup, P.; Davidsen, J.; Jørgensen, K. Lipid Membrane Partitioning of Lysolipids and Fatty Acids: Effects of Membrane Phase Structure and Detergent Chain Length. *J. Phys. Chem. B* **2001**, *105*, 2649−2657.
(57) Kučerka, N.; Nieh, M.-P.; Katsaras, J. Fluid phase lipid areas and bilayer thicknesses of commonly used phosphatidylcholines as a function of temperature. *Biochimica et Biophysica Acta (BBA)-Biomembranes* **2011**, *1808* (11), 2761−2771.
(58) Zhuang, X.; Makover, J. R.; Im, W.; Klauda, J. B. A systematic molecular dynamics simulation study of temperature dependent bilayer structural properties. *Biochimica et Biophysica Acta (BBA)-Biomembranes* **2014**, *1838* (10), 2520−2529.
(59) Wu, E. L.; Qi, Y.; Song, K. C.; Klauda, J. B.; Im, W. Preferred orientations of phosphoinositides in bilayers and their implications in protein recognition mechanisms. *J. Phys. Chem. B* **2014**, *118* (16), 4315−25.
(60) Hall, A.; Róg, T.; Karttunen, M.; Vattulainen, I. Role of glycolipids in lipid rafts: a view through atomistic molecular dynamics simulations with galactosylceramide. *J. Phys. Chem. B* **2010**, *114* (23), 7797−807.
(61) Morell, P.; Radin, N. S. Synthesis of cerebroside by brain from uridine diphosphate galactose and ceramide containing hydroxy fatty acid. *Biochemistry* **1969**, *8* (2), 506−512.
(62) Hall, A.; Róg, T.; Vattulainen, I. Effect of galactosylceramide on the dynamics of cholesterol-rich lipid membranes. *J. Phys. Chem. B* **2011**, *115* (49), 14424−34.
(63) Martinez, D.; Decossas, M.; Kowal, J.; Frey, L.; Stahlberg, H.; Dufourc, E. J.; Riek, R.; Habenstein, B.; Bibow, S.; Loquet, A. Lipid Internal Dynamics Probed in Nanodiscs. *ChemPhysChem* **2017**, *18* (19), 2651−2657.
(64) Dreissig, I.; Machill, S.; Salzer, R.; Krafft, C. Quantification of brain lipids by FTIR spectroscopy and partial least squares regression. *Spectrochimica Acta Part A: Molecular and Biomolecular Spectroscopy* **2009**, *71* (5), 2069−2075.
(65) Alfredsson, V.; Lo Nostro, P.; Ninham, B.; Nylander, T. Morphologies and Structure of Brain Lipid Membrane Dispersions. *Frontiers in cell and developmental biology* **2021**, *9*, 675140.
(66) Mills, T. T.; Huang, J.; Feigenson, G. W.; Nagle, J. F. Effects of cholesterol and unsaturated DOPC lipid on chain packing of saturated gel-phase DPPC bilayers. *General physiology and biophysics* **2009**, *28* (2), 126−139.
(67) Hjort Ipsen, J.; Karlstrom, G.; Mourtisen, O.G.; Wennerstrom, H.; Zuckermann, M.J. Phase equilibria in the phosphatidylcholine-cholesterol system. *Biochimica et biophysica acta* **1987**, *905* (1), 162−172.
(68) Sharma, K. D.; Heberle, F. A.; Waxham, M. N. Visualizing lipid membrane structure with cryo-EM: past, present, and future. *Emerging Topics in Life Sciences* **2023**, *7* (1), 55−65.

https://doi.org/10.1021/jasms.3c00170
J. Am. Soc. Mass Spectrom. 2023, 34, 2006−2015